A Taylor Model Based Description of the Proof Stress of Magnesium AZ31 during Hot Working

M.R. BARNETT

A series of hot-compression tests and Taylor-model simulations were carried out with the intention of developing a simple expression for the proof stress of magnesium alloy AZ31 during hot working. A crude approximation of wrought textures as a mixture of a single ideal texture component and a random background was employed. The shears carried by each deformation system were calculated using a full-constraint Taylor model for a selection of ideal orientations as well as for random textures. These shears, in combination with the measured proof stresses, were employed to estimate the critical resolved shear stresses for basal slip, prismatic slip, $<c + a>$ second-order pyramidal slip, and $\{10\bar{1}2\}$ twinning. The model thus established provides a semianalytical estimation of the proof stress (a one-off Taylor simulation is required) and also indicates whether or not twinning is expected. The approach is valid for temperatures between ~150 °C and ~450 °C, depending on the texture, strain rate, and strain path.

1. INTRODUCTION

SIMPLE constitutive equations describing the flow stress during hot working are often employed in engineering applications where a rapid estimation of the forming load is required. These equations are readily available for widely used metals such as steel and aluminum (*e.g.*, References 1 and 2). With the increase in interest in wrought magnesium products, there is a need for simple descriptions for the flow stress as a function of hot-working conditions. In previous work,[3,4] an expression was developed for the flow stress of magnesium alloy AZ31 at a strain of 0.5:

$$\sigma_{0.5} = 90 \sin h^{-1}\left(\frac{Z}{10^{13}}\right)^{0.15} \quad [1]$$

where Z is the Zener–Hollomon parameter ($Z = \dot{\varepsilon} \exp(147{,}000/RT)$) and R is the gas constant. This expression provides an approximate value for the flow stress for uniaxial and channel-die compression that is relatively insensitive to texture (because, by a strain of 0.5, a stable compression texture has been attained). At the proof stress and in the initial work-hardening region, however, the effect of texture is more marked, and a more complex expression is required.[3] The present work is concerned with the development of such an equation for the hot-working proof stress of magnesium alloy AZ31.

The change in proof (or yield) stress of AZ31 sheet in tension as a function of temperature and strain rate has been studied since at least the 1950s (*e.g.*, Reference 5), and data relating to the phenomenon appear in a number of magnesium design handbooks (*e.g.*, Reference 6). Some of these data were examined by Takuda *et al.*,[7] who concluded that a logarithmic stress law based on the Zener–Hollomon parameter is appropriate for this deformation mode. A limited set of results for extruded material tested in compression has also been published,[6] but these do not appear to have been subjected to any significant analysis. It is well known, however, that there is a difference in the proof stresses of extrusions tested in compression along the extrusion axis and those tested in tension along the same axis, particularly at lower temperatures. The yield stress in tension is typically twice that in compression. This general observation arises from the strong crystallographic texture and the activation of twinning in the compression tests (*e.g.*, Reference 8).

Recent work by Agnew *et al.*,[9] along with previous studies by Phillipe,[10] has shown that both the room-temperature anisotropy of flow stress and the texture can be simulated to a fairly satisfactory level using crystal-plasticity models. One of the challenges with these models is arriving at appropriate input values for the critical resolved shear stresses (τ_i) for the separate deformation systems. In the present work, we are concerned with the effect of temperature, which, as illustrated in Figure 1, on τ_i is significant.[9,11–18] The systems represented in this figure reflect the main deformation modes believed to be important in magnesium, but there are certainly others, such as $\{10\bar{1}1\}$ twinning.[16] A temperature-insensitive critical stress of ~4 τ_{basal} is shown for $\{10\bar{1}2\}$ twinning based on the present work and References 9 and 16 through 18, although the validity of this estimate has not been clearly demonstrated.

Figure 1 shows that in the hot-working regime ($T >$ ~$0.6T_m$, which is equivalent to $T >$ ~280 °C for Mg), the variation of the critical resolved shear stresses amongst the different deformation modes is considerably lower than at room temperature. This means that hot deformation is more suited to the application of fully constrained Taylor-type simulation. Deformation at lower temperatures, where the values of key critical resolved shear stresses are quite disparate, is better simulated with self-consistent-type models.[9] However, Phillipe[10] has had some success in applying Taylor-type simulations to this situation.

A framework is presented here for a simple approximation of the texture and for an estimation of its impact on the proof stress based on Taylor-type crystal-plasticity considerations. The basic idea is to establish key parameters in a simple

M.R. BARNETT, Senior Research Fellow, is with the CRC for Cast Metals Manufacturing, School of Engineering and Technology, Deakin University, Geelong, VIC 3217, Australia. Contact e-mail: barnettm@deakin.edu.au

Manuscript submitted October 10, 2002.

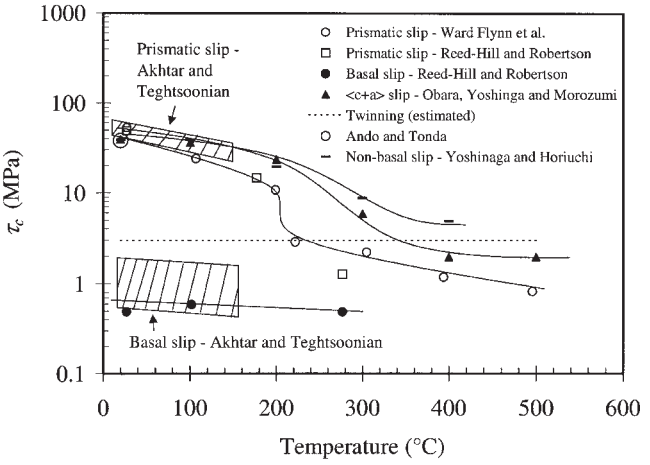

Fig. 1—Influence of deformation temperature on the critical resolved shear stress.[9–18]

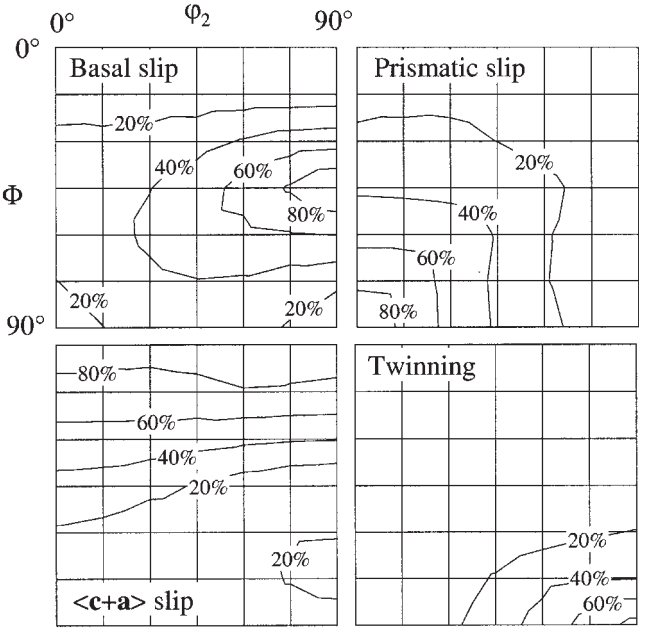

Fig. 2—The influence of orientation on the fraction of the total shears born by the different deformation systems, calculated using a full constraint Taylor model and setting τ_{basal}: $\tau_{prismatic}$: $\tau_{<c+a>}$: $\tau_{twinning}$ = 1:10:10:4.

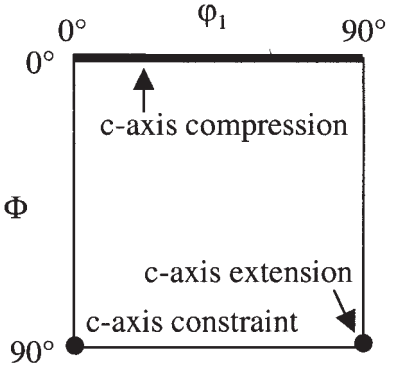

Fig. 3—The relationship between deformation and the *c*-axis in plane-strain deformation shown using ODF representation (Bunge convention). This holds true for all values of φ_2.

equation using a one-off Taylor simulation. The intent is to generate an equation that can be used in an analytical manner, without the need for further crystal-plasticity simulation. Following this, a number of experimental data describing the influence of texture, strain path, strain rate, and temperature on the hot-working proof stress are presented. These are then analyzed in terms of the simple model developed in the earlier sections.

II. BACKGROUND AND MODEL OUTLINE

A full-constraint Taylor-type model, which lends itself readily to generating the simplified expression desired in the present work, was employed to examine the influence of the critical resolved shear stresses on system activity and deformation stress. This model configuration is "rigid," in that it imposes the same strain on each grain and calculates the five shears that satisfy this strain for the minimum expended internal work. Four deformation systems were used in the model: basal slip, prismatic slip, $<c+a>$ second-order pyramidal slip ($\{11\bar{2}2\}<\bar{1}\bar{1}23>$), and $\{10\bar{1}2\}$ tension twinning. The activity of each system is determined by the model. System activity is expressed here as the shear on the system divided by the strain in the direction along which the stress is applied ($d\gamma_i/d\varepsilon$).

To illustrate the influence of texture on deformation-system activity, results from an initial simulation of plane-strain deformation (*i.e.*, channel-die compression) are presented in Figure 2. The critical stresses employed in the simulation correspond approximately to those expected for intermediate temperatures in Figure 1 (*i.e.*, τ_{basal}: $\tau_{prismatic}$: $\tau_{<c+a>}$: $\tau_{twinning}$ = 1:10:10:4). The plots show the percentage of the total shear born by each system as a function of the Euler angles φ_1 and Φ, averaged over φ_2. A legend for the orientation distribution function (ODF) representation used in this work is given in Figure 3. The Bunge-convention Euler angle, Φ, refers to the inclination of the hcp *c*-axis to the primary compression direction. The term φ_1 refers to the direction in which the *c*-axis is tilted (φ_1 = 90 deg for tilting in the extension direction and φ_1 = 0 deg for inclination in the direction of constraint). The term φ_2 indicates the degree to which the unit cell is rotated around the *c*-axis once the other two rotations have been performed. The relative activities of the various slip modes are shown to be reasonably insensitive to φ_2. Thus, it is convenient to average the predictions over this parameter.

The plots in Figure 2 show that, when the *c*-axis is aligned with the compression direction, the deformation is expected to be accommodated largely by $<c + a>$ slip. When the *c*-axis is aligned with the extension direction, twinning is favored, and when the *c*-axis is constrained, prismatic slip is expected to be prolific. Due to the "rigidity" of the Taylor model, these predictions understate the role of basal slip. They are, nevertheless, in reasonable agreement with experimental observations (*e.g.*, Reference 19) and form a useful guide to system activity.

In addition to crystal orientation, the magnitude of the critical resolved shear stress for a given deformation system,

relative to the other systems, influences its degree of activity. However, for the present model, a simplified description of this effect is required. Fortunately, there are two principles that permit such a simplification to be made. One is that data from the literature (Figure 1) for the relative critical resolved shear stresses can be readily idealized. As a first approximation, $\tau_{\text{prismatic}}$ can be set equivalent to $\tau_{<c+a>}$ and both τ_{twinning} and τ_{basal} can be considered to be relatively insensitive to temperature with $\tau_{\text{twinning}} \sim 4\tau_{\text{basal}}$. The other arises from the geometry of slip, according to which the influence of critical resolved shear stress on system activity is not necessarily continuous. For instance, the only deformation system, among the four considered here, that gives rise to any compression along the *c*-axis is the pyramidal $<c + a>$ slip system. Therefore, whenever compression is imposed along the *c*-axis, the full-constraint Taylor model used in this work requires the activation of this system, irrespective of the value of its relative critical stress.

The most significant effect of critical resolved shear stress on system activity seen in the present simulations is in the activation of $\{10\bar{1}2\}$ twinning. The amount of twinning predicted by the Taylor model shows a significant and sharp transition with changing $\tau_{<c+a>}$: τ_{twinning} ratio in deformations involving *c*-axis extension. This is illustrated in Figure 4 for simulations based on experimental channel-die test textures (Figure 7). The transition can be explained by a combination of two factors. One is the change in relative magnitude of the critical stresses for $\{10\bar{1}2\}$ twinning and $<c + a>$ slip with increasing temperature. The other is that for *c*-axis extension, the geometry places these two systems in direct competition with each other. This phenomenon is a specific case of the transition from twinning to slip that occurs in many alloy systems when the temperature is increased or the strain rate is decreased.[17]

The fact that deformation-system activity plays a role in determining the proof stress suggests that a change in deformation stress may occur at the slip-twinning transition point. This is illustrated in Figure 5, which displays the deformation stress calculated from the Taylor simulations using the following expression:

$$\sigma = \frac{d\gamma_{\text{basal}}}{d\varepsilon}\tau_{\text{basal}} + \frac{d\gamma_{\text{prismatic}}}{d\varepsilon}\tau_{\text{prismatic}} + \frac{d\gamma_{<c+a>}}{d\varepsilon}\tau_{<c+a>} + \frac{d\gamma_{\text{twinning}}}{d\varepsilon}\tau_{\text{twinning}} \quad [2]$$

A clear kink in the stress *vs* τ_{nonbasal} curve can be seen in the results for the *c*-axis extension texture, where a marked twinning-slip transition occurs. Otherwise, the deformation stress varies linearly with τ_{nonbasal}.

Based on these considerations, the influence of critical resolved shear stress on system activity considered in the present model is restricted to the slip-twinning transition. That is, only two separate regimes of system activity are considered, one corresponding to high values of the ratio of $\tau_{<c+a>}$: τ_{twinning}, where $\{10\bar{1}2\}$ twinning is allowed, and one at low values of this ratio, where $\{10\bar{1}2\}$ twinning does not occur.

In addition to an abbreviated description of the deformation-system activity, the present objective of generating a simple proof-stress equation requiring only a one-off Taylor simulation needs a lean description of the texture. One simplification has already been introduced previously, where the simulation results were averaged over φ_2. Another way of putting this is that the position of the *c*-axis with respect to

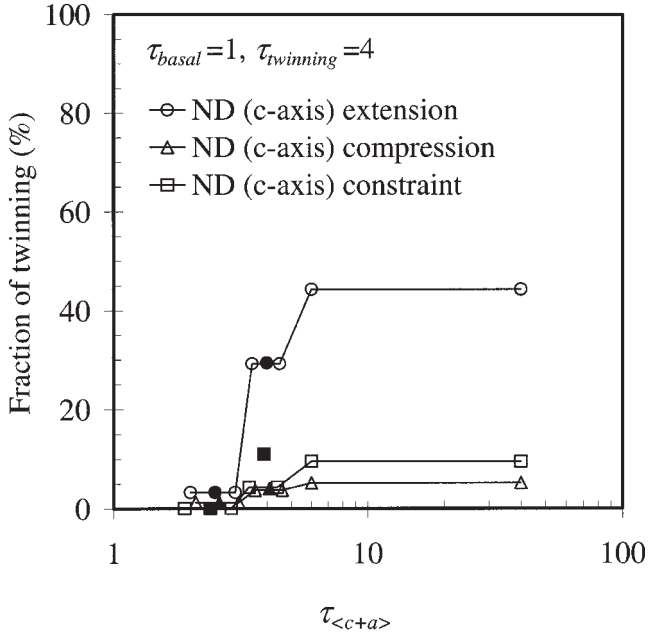

Fig. 4—Influence of $\tau_{<c+a>}$ on the fraction of twinning calculated for the three main present channel die textures (discretized into 50 orientations). Open symbols, $\tau_{\text{prismatic}} = \tau_{<c+a>}$; and filled symbols, $\tau_{\text{prismatic}} = 2\tau_{<c+a>}$. Note the large change in the fraction twinning for the case of ND (*c*-axis) extension.

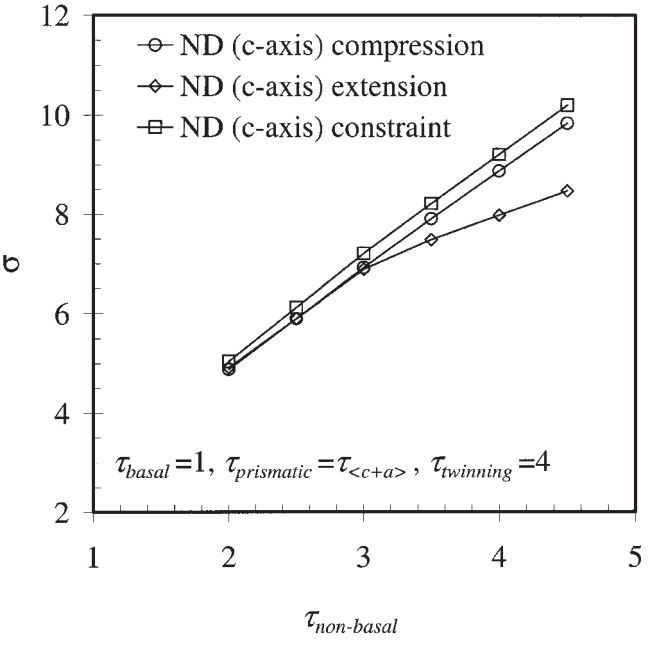

Fig. 5—Influence of the critical resolved shear stress for nonbasal slip on the expected deformation stress in plane-strain deformation for the simulations shown in Fig. 4. Note the kink in the ND (*c*-axis) extension case, which is caused by the slip-twinning transition.

the reference-system axes is the key to the mechanical anisotropy (*e.g.*, Reference 19). The description of magnesium textures is made even easier by the fact that most of the textures in wrought products consist, to a first approximation, of a single fiber based on the orientation of the *c*-axis. In rolling, the *c*-axis is largely found close to the normal direction (ND), and in extrusion, it lies perpendicular to the extrusion direction and generally normal to the extrudate surface.

The texture of magnesium is, therefore, described here as a combination of an ideal component and a random component. The volume fraction of material represented by the ideal component is taken as the fraction (x) of material with a *c*-axis within 20 deg of the key principal direction in question. Equation [2] can then be rewritten as:

$$\sigma = \sum_{i=1}^{4} \left(x \frac{d\gamma_i^{\text{ideal}}}{d\varepsilon} + (1 - x) \frac{d\gamma_i^{\text{random}}}{d\varepsilon}\right)\tau_i \qquad [3]$$

where i refers to the deformation system.

Values of $d\gamma_i/d\varepsilon$ for ideal orientations and random textures were calculated using the Taylor model for a number of common strain paths and textures. This was carried out for the two regimes of system activity considered in the model: an idealized twinning region (characterized by τ_{basal}: $\tau_{\text{prismatic}}$: $\tau_{<c+a>}$: τ_{twinning} = 1:30:30:4) and an idealized slip-only region (characterized by τ_{basal}: $\tau_{\text{prismatic}}$: $\tau_{<c+a>}$: τ_{twinning} = 1:2:2:4). The results are presented in Tables I and II.

Equation [3] was employed, in combination with the values in Table II for the slip-only region, to predict the yield stress of artificial (Gaussian) *c*-axis compression textures of varying intensities. The results are compared in Figure 6 with those generated using Taylor simulations based on the complete texture. There is reasonable agreement, and, while the simplified texture description will be obviously limited, its applicability to *c*-axis compression-type textures is important, as this situation is frequently encountered in forging, rolling, extrusion, and tensile deformation of sheet metals.

III. MODEL APPLICATION

A. *Experimental Results*

The magnesium alloy AZ31, the nominal composition of which is 3 wt pct Al and 1 wt pct Zn with a minimum Mn content of 0.2 wt pct, was received in the as-extruded state. A pole-figure representation of the texture of the bar is given in Figure 7. Of the orientations in this sample, 90 pct contained a *c*-axis within 20 deg of the normal to the extrusion direction. Samples of the 19-mm-diameter bar (grain size of 23 μm) were machined into torsion and uniaxial compression specimens. The axial direction of the machined samples corresponded to the axial direction of the extruded bar. A section of bar was hot rolled at 350 °C into a 10 mm plate and then annealed at 350 °C for one hour. From this sample, three differently oriented channel-die specimen types were cut.[3] One set of samples was oriented such that the compression occurred in the direction corresponding to the rolling ND. Another set was oriented for extension in the rolling ND. The third orientation was such that the rolling ND was constrained during deformation. The orientation distribution function rep-

Table I. Distribution of the Shears among the Different Systems for the {10$\bar{1}$2} Twinning Region for Key Texture Components (Calculated Using a Full-Constraint Taylor Model with τ_{basal}: $\tau_{\text{prismatic}}$: $\tau_{<c+a>}$: τ_{twinning} = 1:30:30:4)

		$\sum \frac{d\gamma_i}{d\varepsilon}$	$\frac{d\gamma_{\text{basal}}}{d\varepsilon}$	$\frac{d\gamma_{\text{prismatic}}}{d\varepsilon}$	$\frac{d\gamma_{<c+a>}}{d\varepsilon}$	$\frac{d\gamma_{\text{twinning}}}{d\varepsilon}$
Plane strain	random	3.02	1.12	1.06	0.33	0.51
	c-axis = compression direction	2.60		0.34	2.26	
	c-axis = extension direction	2.38		0.36		2.02
	c-axis = constraint direction	2.22		2.22		
Uniaxial compression	random	2.58	0.75	0.83	0.59	0.41
	c-axis = radial direction	2.26		1.24	0.00	1.02
Tensile	random	2.49	0.67	0.80	0.45	0.57
	c-axis = radial direction	2.38		1.26	1.12	

Table II. Distribution of the Shears among the Different Systems for the Slip Only Region for Key Texture Components (Calculated Using a Full-Constraint Taylor Model with τ_{basal}: $\tau_{\text{prismatic}}$: $\tau_{<c+a>}$: τ_{twinning} = 1:2:2:4)

		$\sum \frac{d\gamma_i}{d\varepsilon}$	$\frac{d\gamma_{\text{basal}}}{d\varepsilon}$	$\frac{d\gamma_{\text{prismatic}}}{d\varepsilon}$	$\frac{d\gamma_{<c+a>}}{d\varepsilon}$	$\frac{d\gamma_{\text{twinning}}}{d\varepsilon}$
Plane strain	random	2.94	1.00	1.03	0.91	
	c-axis = compression direction	2.60		0.34	2.26	
	c-axis = extension direction	2.60		0.34	2.26	
	c-axis = constraint direction	2.22		2.22	0.00	
Uniaxial compression	random	2.53	0.66	0.81	1.06	
	c-axis = radial direction	2.37		1.26	1.11	
Tensile	random	2.53	0.66	0.81	1.06	
	c-axis = radial direction	2.38		1.26	1.12	

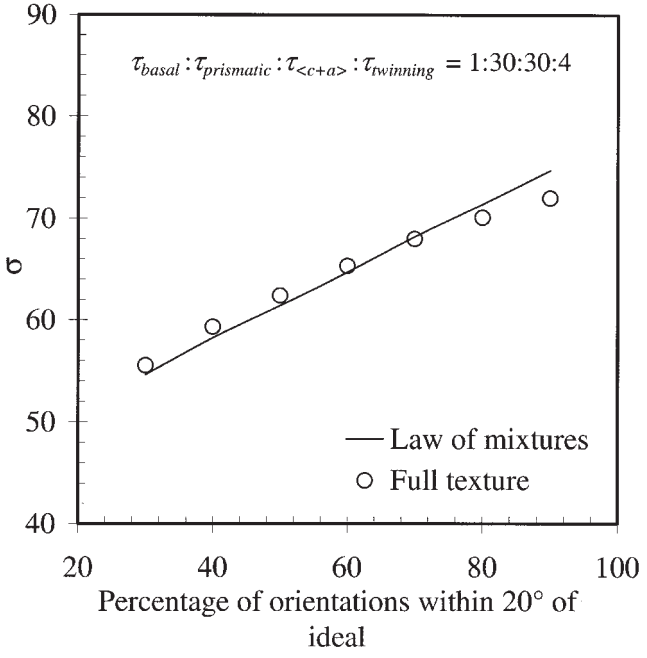

Fig. 6—Influence of the intensity of textures in plane strain oriented for ND (*c*-axis) compression. The textures used were generated artificially by placing a Gaussian peak of varying sharpness on the ideal *c*-axis compression component. Agreement is evident between stress calculations made using the entire texture and those based on a law-of-mixture approximation of the texture (refer to text).

resentation of these textures, averaged over φ_2 and described in the channel-die reference frame, is presented in Figure 7. Of all the orientations present in these samples, 40 pct contained a *c*-axis within 20 deg of the rolling ND.

Isothermal constant-strain-rate hot-deformation tests were carried out at temperatures between 250 °C and 450 °C and at strain rates between 0.001 and 1 s^{-1}. The samples were heated directly to the test temperature and held for approximately 5 minutes prior to testing, to equalize the temperature. The proof stress was calculated according to the 0.2 pct offset method.

The stress-strain curves measured in these tests are given in full elsewhere,[3] so only the data obtained for some of the uniaxial compression tests are presented here (Figure 8). It can be seen that with decreasing temperature, the shape of the flow curve changes, and this can be attributed to the onset of twinning.[3,20] The true proof stresses measured in the different compression tests are given in Figure 9 as a function of strain rate at 300 °C. In the samples oriented such that a majority of grains experienced *c*-axis extension, the stress levels off at high strain rates. This behavior can also be explained in terms of the onset of twinning (Figure 5) and coincides with the change in flow-curve shape illustrated in Figure 8. The proof stresses measured in the ND (*c*-axis) – constraint channel-die compression tests (T = 300 °C to 400 °C and $\dot{\varepsilon}$ = 0.001 to 0.1 s^{-1}) are presented in Figure 10 as a function of the Zener–Hollomon parameter (Q = 147,000 J/mol).*

*In magnesium, the effective activation energy for deformation (Q) is actually a function of temperature, but it has been found that an average value of 147,000 J/mol can be employed for the present purpose.[3]

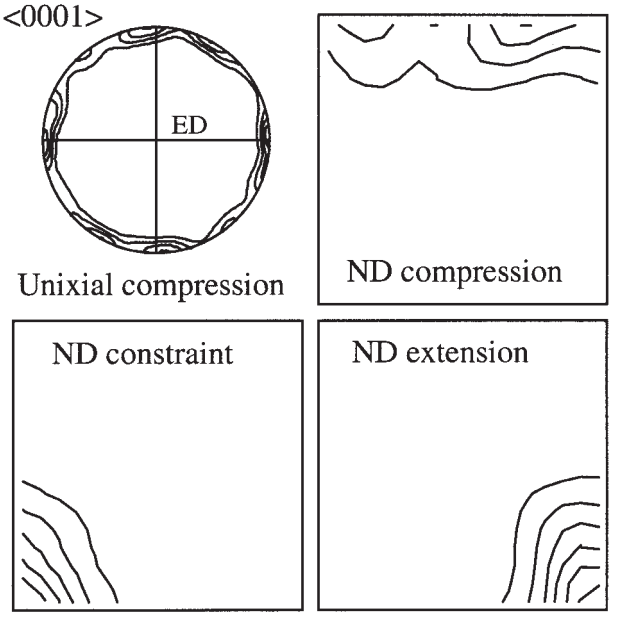

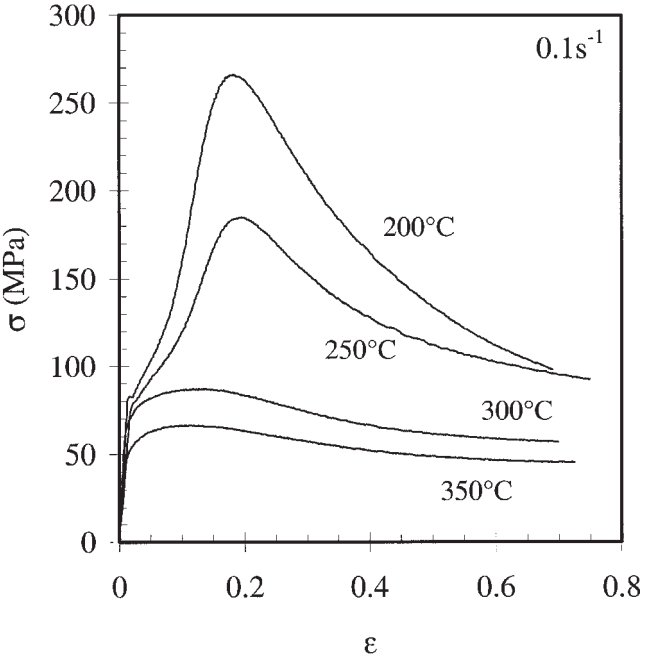

Fig. 8—True stress-strain curves measured in uniaxial compression along the extrusion direction. The distinctive change in curve shape with decreasing temperature between 300 °C and 250 °C is due to the activation of twinning in the lower-temperature tests.

B. *Model Parameters*

In the following, the model is completed by generating estimates for the values of the critical resolved shear stresses at the proof stress using Eq. [3] and the shears presented in Tables I and II.

With reference to Figure 2, it is evident that prismatic slip predominates in plane strain when the *c*-axis is constrained, something that occurs to a large degree in channel-die testing of rolled material when the rolling ND

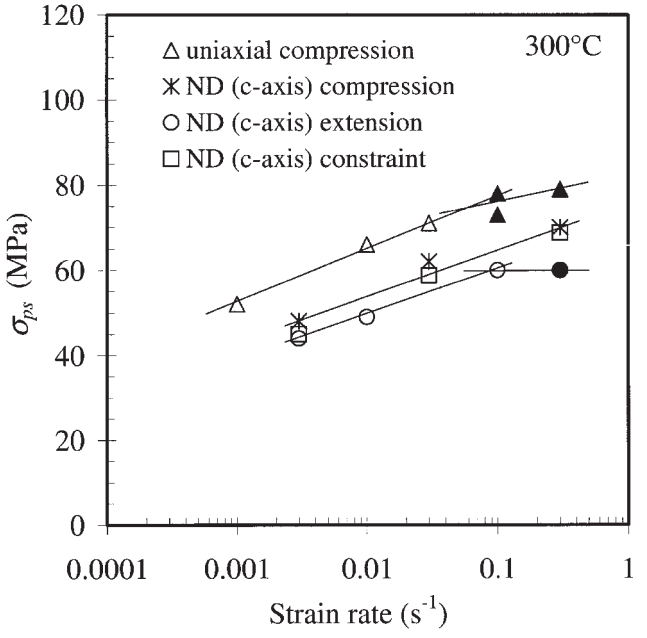

Fig. 9—Influence of the strain rate on the 0.2 pct proof stress. Filled symbols indicate the flow curves were typical of samples in which twinning occurs. Note the different stress levels for the different samples and the inflexion in the data for the uniaxial compression and the ND (*c*-axis) extension channel die samples.

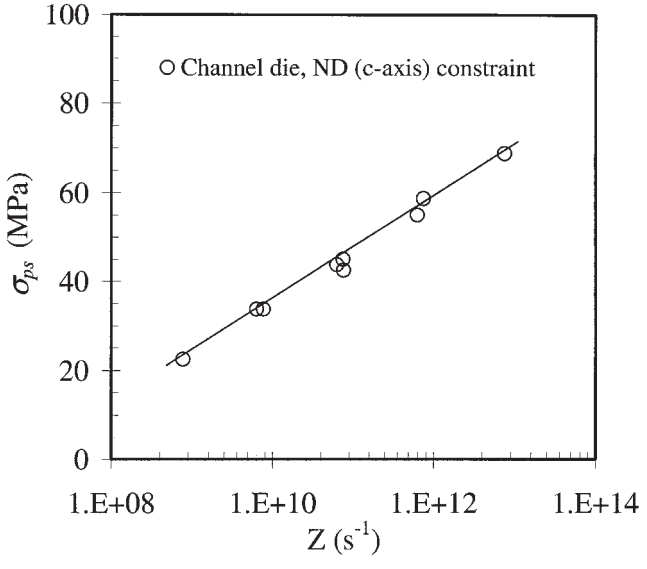

Fig. 10—Influence of Z (Q = 147,000 kJ/mol) on the proof stress of channel die samples oriented for ND (*c*-axis) constraint (T = 300 °C to 400 °C and $\dot{\varepsilon}$ = 0.001 s^{-1} to 0.1 s^{-1}).

is constrained. When the *c*-axis is compressed (*e.g.*, in channel-die tests of rolled material compressed along the rolling ND), second-order pyramidal slip dominates. The similarity of the proof stresses obtained under these two conditions for different strain rates (Figure 9) suggests that a relatively constant ratio, $f_{<c+a>}$, exists between $\tau_{\text{prismatic}}$ and $\tau_{<c+a>}$. Equating versions of Eq. [3] for these two situations and rearranging gives the following expression (for a constant $d\varepsilon$):

$$f_{<c+a>} = \frac{\tau_{<c+a>}}{\tau_{\text{prismatic}}} = -\frac{d\gamma^{\text{c-const.}}_{\text{prismatic}} - d\gamma^{\text{c-comp.}}_{\text{prismatic}}}{d\gamma^{\text{c-const.}}_{<c+a>} - d\gamma^{\text{c-comp.}}_{<c+a>}} \quad [4]$$

where the superscripts refer to the ideal texture components. Using the values in Table II for the slip-only region yields a value for $f_{<c+a>}$ of 0.83. This is roughly in line with the data in Figure 1, which show τ_i to be similar for these two systems.

To establish the magnitude of the critical stress for twinning, a similar set of simultaneous equations can be solved for the stress which corresponds to the characteristic kink σ_{kink} in the stress *vs* strain-rate curves for samples orientated for *c*-axis extension. In this case, Eq. [3], based on the shears calculated for the twinning region (Table I), is equated with the same expression for shears calculated for the slip-only region (Table II). The resulting expression is

$$\tau_{\text{twinning}} = \sigma_{\text{kink}}\left(\frac{d\varepsilon}{d\gamma^{\text{twin}}_{\text{twinning}}} - \frac{f_{basal}\, d\gamma^{twin}_{basal} \Big/ d\varepsilon}{f_{basal}\, d\gamma^{no\text{-}twin}_{basal} \Big/ d\varepsilon} \right. \quad [5]$$

$$\left. \frac{+\, d\gamma^{\text{twin}}_{\text{prismatic}} \Big/ d\varepsilon + 0.83\, d\gamma^{\text{twin}}_{<c+a>} \Big/ d\varepsilon}{+\, d\gamma^{\text{no-twin}}_{\text{prismatic}} \Big/ d\varepsilon + 0.83\, d\gamma^{\text{no-twin}}_{<c+a>} \Big/ d\varepsilon} \right)$$

where, in this case, the superscripts refer to whether the shears are calculated for the slip-only (no twinning) or twinning regions, and f_{basal} is the magnitude of τ_{basal} in terms of $\tau_{\text{prismatic}}$. The term f_{basal} is expected to take a value in the range 0.1 to 0.2 at intermediate temperatures, as shown in Figure 1. The mean values of τ_{twinning} thus calculated for the channel-die and the two sets of uniaxial compression data are 27, 33, and 36 MPa. These values vary by ~1 MPa over the expected range of f_{basal} given previously; thus, the exact value of f_{basal} is not critical in this instance. The range of values obtained for τ_{twinning} reflects, in part, the approximations inherent in the present technique and the difficulty in identifying the value of σ_{kink}. For the current purposes, an average value of 32 MPa is assumed. The values for τ_{basal} obtained in this analysis fall between 3.3 and 7.4 MPa. For ease of calculation, a temperature-insensitive value for τ_{basal} of 5 MPa is adopted. This also consistent with the relatively athermal behavior of basal slip evident in Figure 1.

Now that we have established values for $\tau_{\text{c,basal}}$ (5 MPa), $f_{<c+a>}$ (0.83), and τ_{twinning} (32 MPa), it is a fairly straight forward matter to rearrange Eq. [3] to obtain a value for $\tau_{\text{prismatic}}$ based on a measured proof stress. It now remains to relate these values to the strain rate and temperature of hot deformation. Accordingly, Figure 11 shows a plot of $\tau_{\text{prismatic}}$ against Z for data obtained in the slip-only region. Reasonable agreement amongst the results is evident, and the data are grouped around a logarithmic stress law:

$$\tau_{\text{prismatic}} = 2.5 \ln(Z) - 38 \quad [6]$$

The values for τ_i and $d\gamma_i/d\varepsilon$ established here (Tables I through III), in conjunction with Eq. [3], form a model for the proof stress based on the texture and deformation conditions. The values for $d\gamma_i/d\varepsilon$ employed depend on whether deformation is performed within the twinning regime or not.

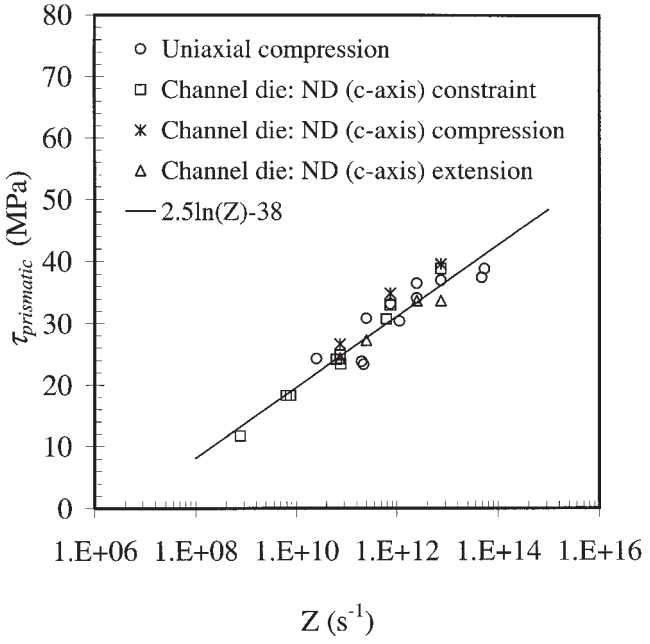

Fig. 11—Influence of Z (Q = 147,000 kJ/mol) on the critical resolved shear stress for prismatic slip. These values were obtained using the measured proof stress and Eq. [3] by assigning τ_{basal} = 5 MPa, $\tau_{twinning}$ = 32 MPa, and $\tau_{<c+a>} = 0.83\ \tau_{prismatic}$.

Table III. Model Parameters Determined from Experiment

Parameter	Value
τ_{basal}	5 MPa
$\tau_{prismatic}$	2.5 ln (Z)–38 MPa
$\tau_{<c+a>}$	2.1 ln (Z)–32 MPa
$\tau_{twinning}$	32 MPa
Twinning region	$Z > 7 \times 10^{12}\ s^{-1}$

The active regime is the one that produces the lowest stress for a given condition. Inspection of Tables I and II shows that the differences between the predicted shears for the twinning and slip-only regions lie predominantly with the twinning and $<c + a>$ slip modes. This is expected, because these are the only two modes that give c-axis extension. A ratio of the two critical resolved shear stresses ($\tau_{<c+a>}/\tau_{twinning}$) can, therefore, be used to mark the transition point. Using the value of τ_{basal} determined previously and the shears given in Tables I and II, values for this ratio can be calculated for the different strain paths and textures. The results of these calculations fall between 0.9 and 0.97. This range is relatively small given the spread of textures, and its tightness can be ascribed to the similar orientation of the shear directions and normals for these two systems. If a texture-insensitive value of 0.93 is assumed, it can be readily established, using Eq. [6] and values for $\tau_{twinning}$ and $f_{<c+a>}$, that twinning should be activated if the Zener–Hollomon parameter exceeds a critical value, irrespective of the texture. In the present case, this value is $\sim 7 \times 10^{12}\ s^{-1}$.

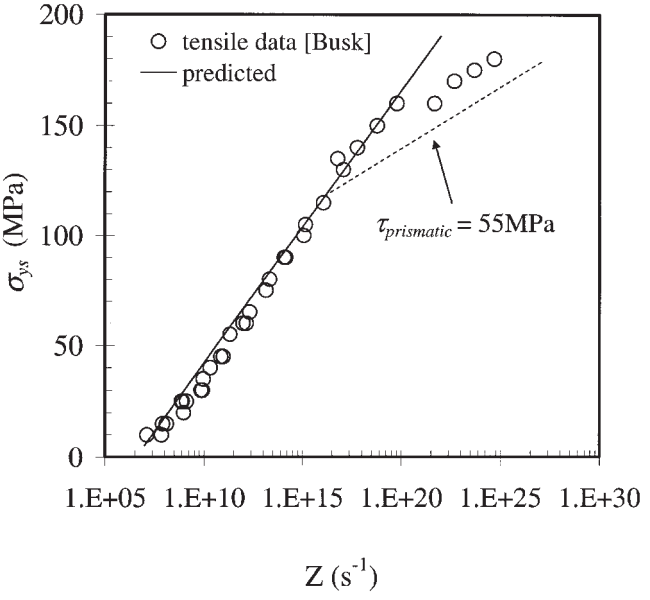

Fig. 12—Influence of Z on the proof stress measured in tension tests carried out on extruded bar[6] showing agreement with the present model, which was derived using compression tests.

IV. DISCUSSION

The values of the critical resolved shear stress for prismatic slip obtained by inverting the current model show a reasonable correlation with the Zener–Hollomon parameter over the range of 10^9 to $10^{14}\ s^{-1}$. This suggests that the present model should be applicable to deformations carried out in the temperature range of 210 °C to 430 °C (for a strain rate of 0.01 s^{-1}). The lower limit of this temperature range corresponds to a homologeous temperature of approximately 0.5, which is just below typical hot-working temperatures ($T > 0.6T_m$). Some caution must be taken, however, in applying the current model to these lower temperatures, as it is in this region that key assumptions inherent in the present approach start to break down.

As mentioned previously, the Taylor model employed in the present work imposes the same strain on all grains. In reality, the strain is distributed differently within grains and amongst grains. The effect of the latter becomes increasingly important with a high anisotropy of plastic deformation (*i.e.*, widely differing values of the critical resolved shear stresses for different deformation modes). Figure 1 shows that there is a marked increase in the anisotropy of deformation in magnesium as the temperature of deformation is lowered. A particular outcome of this is that the "softer" deformation modes (particularly basal slip) will increase in their activity. This effect is not captured in the present model, due to the rigid Taylor formulation employed and the consideration of only two regimes of slip activity.

The application of the present model to both tension and lower-temperature deformations is illustrated in Figures 12 and 13. In Figure 12 it can be seen that the model describes the tensile proof stress of an extruded bar (data from Reference 5) fairly well for values of the Zener–Hollomon parameter up to $\sim 10^{20}\ s^{-1}$. The agreement with such high values of Z is somewhat surprising. In this instance, in which $\{10\bar{1}2\}$ twinning does not play a role and where $<c + a>$

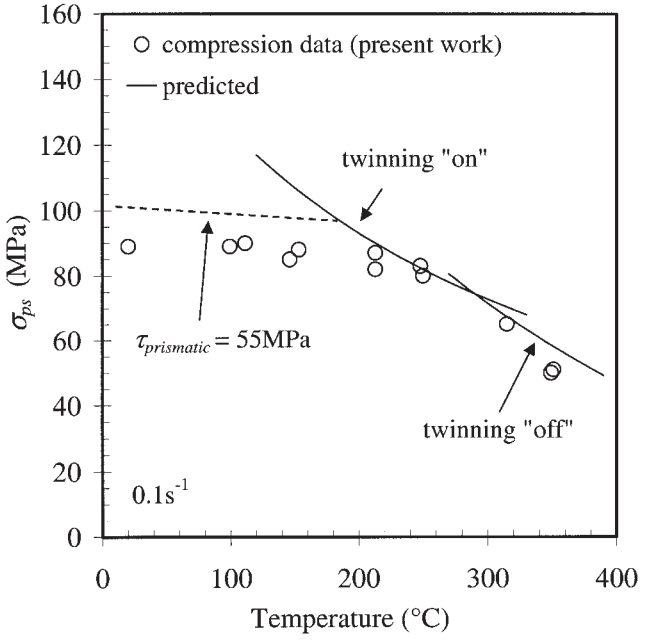

Fig. 13—Comparison between model and experimental values for the proof stress in uniaxial compression.

slip is important, the model can be applied to deformation at temperatures as low as 100 °C (for a strain rate of 0.15^{-1}).

In uniaxial compression of an extruded bar, the roles of twinning and prismatic slip become more important, and the breakdown of the model at low temperatures is more noticeable (Figure 13). In this case, it can be seen that the model overpredicts the proof stress at temperatures less than ~200 °C. While this reflects the limitations of the present model discussed previously, it is also consistent with the suggestion made recently[21] that $f_{<c+a>}$ increases with decreasing temperature for temperatures between ~25 °C and ~200 °C. If it is assumed that, for deformation below 200 °C, the critical resolved shear stress for $\tau_{\text{prismatic}}$ is held constant at 55 MPa while the other values of τ_i remain as before, the proof stresses shown as dashed lines in Figures 12 and 13 are obtained. This modification brings predictions into closer alignment with the experiment, which suggests that the change in $f_{<c+a>}$ with temperature is indeed important at low temperatures. The remaining discrepancy between the model and experiment can be explained by the issues discussed above and the possible action of other twinning modes.[13]

In general, the values of the critical resolved shear stresses obtained in the present work vary in a roughly similar ratio (τ_{basal}: $\tau_{\text{prismatic}}$: $\tau_{<c+a>}$: τ_{twinning} ~ 1:6:5:6) for intermediate hot-working conditions. The actual values are 2 to 3 times greater in magnitude compared to Figure 1, and this difference can be ascribed to the influence of solute elements and polycrystalline strengthening.

V. CONCLUSIONS

Simplified descriptions of common textures and the critical resolved shear stresses were employed to develop an analytical expression for the proof stress of magnesium alloy AZ31 during hot working. The expression holds for deformation between ~150 °C and 450 °C, depending on the strain rate, texture, and strain path.

For the present purposes, the texture can be effectively described using a law-of-mixtures approach that combines a random array of orientations and a single ideal component.

The model was inverted to derive the following approximate values for the critical resolved shear stresses of magnesium alloy AZ31: $\tau_{\text{basal}} = 5$ MPa, $\tau_{\text{twinning}} = 32$ MPa, $\tau_{\text{prismatic}} = 2.5 \ln(Z) - 38$, and $\tau_{<c+a>} = 2.1 \ln(Z) - 32$.

It was shown that $\{10\bar{1}2\}$ twinning is activated when deformation is carried out above a critical value of the Zener–Hollomon parameter, which in this case is $\sim 7 \times 10^{12}$ s^{-1}.

ACKNOWLEDGMENTS

The support of the French Embassy Scientific Fellowship scheme is gratefully acknowledged for the portion of the present work that was carried out at the Ecole National Superieur des Mines de Saint-Etienne. The CRC for Cast Metals Manufacturing was established under the Australian government's Co-operative Research Grants scheme.

REFERENCES

1. J.J. Jonas, C.M. Sellars, and W.J.McG. Tegart: *Metall. Rev.*, 1969, pp. 1-24.
2. A. Lasraoui and J.J. Jonas: *Metall. Trans. A*, 1991, vol. 22A, pp. 1545-58.
3. M.R. Barnett: *J. Light Met.*, 2001, vol. 1, pp. 167-77.
4. M.R. Barnett: *Proc. Int. Conf. on Thermomechanical Processing: Mechanics, Microstructure & Control*, Sheffield, United Kingdom, June 2002, in press.
5. R.S. Busk: *Magnesium Products Design*, Marcel Dekker, New York, NY, 1987, p. 387.
6. *ASM Speciality Handbook: Magnesium and Magnesium Alloys*, M.M. Avedesian and H. Baker, eds. ASM INTERNATIONAL, Materials Park, OH, 1999, p. 177.
7. H. Takuda, H. Fujimoto and N. Hatta: *J. Mater. Proc. Technol.*, 1998, vol. 80–81, pp. 513-16.
8. E.A. Ball and P.B. Prangnell: *Scripta Metall. Mater.*, 1994, vol. 31, 1994, pp. 111-16.
9. S.R. Agnew, M.H. Yoo, and C.N. Tomé: *Acta Mater.*, 2001, vol. 49, pp. 4277-89.
10. M.J. Phillipe: *Rev. Metall.–CIT*, 1998, Dec., pp. 1491-99.
11. T. Obara, H. Yoshinga, and S. Morozumi: *Acta Metall.*, 1973, vol. 21, pp. 845-53.
12. P. Ward Flynn, J. Mote, and J.E. Dorn: *Trans. TMS-AIME*, 1961, vol. 221, pp. 1148-54.
13. R.E. Reed-Hill and W.D. Robertson: *Acta Metall.*, 1957, vol. 5, pp. 728-37.
14. S. Ando and H. Tonda: *Mater. Trans. JIM*, 2000, vol. 41, pp. 1188-91.
15. H. Yoshinaga and R. Horiuchi: *Trans. JIM*, 1963, vol. 4, pp. 1-8.
16. B.C. Wonsiewicz and W.A. Backofen: *Trans. TMS-AIME*, 1967, vol. 239, pp. 1422-31.
17. M.A. Meyers, O. Vohringer, and V.A. Lubarda: *Acta Mater.*, 2001, vol. 49, pp. 4025-39.
18. M.A. Gharghouri, G.C. Weatherly, J.D. Embury, and J. Root: *Phil. Mag. A*, 1999, vol. 79, pp. 1671-95.
19. E.W. Kelley and W.F. Hosford: *Trans. TMS-AIME*, 1968, vol. 242, pp. 654-60.
20. R. Gehrmann and G. Gottstein: *Proc. 12th Int. Conf. on Textures of Materials*, J.A. Szpunar, ed., NRC Research Press, Montreal, 1999, pp. 665-70.
21. S.R. Agnew and O. Duygulu: *Mater. Sci. Forums*, 2003, vol. 419–422, pp. 177-82.